CHEMISTRY
A EUROPEAN JOURNAL

DOI: 10.1002/chem.201000144

Rapid Epitaxial Growth of Ag on Au Nanoparticles: From Au Nanorods to Core–Shell Au@Ag Octahedrons

Ana Sánchez-Iglesias, Enrique Carbó-Argibay, Arnaud Glaria, Benito Rodríguez-González, Jorge Pérez-Juste, Isabel Pastoriza-Santos,* and Luis M. Liz-Marzán[a]

The strongly shape-dependent optical properties of metal nanoparticles have motivated the rapid development of new and efficient strategies toward morphology control.[1–3] However, a highly efficient control over shape and size has been mainly achieved for gold. Therefore, an interesting route toward the production of other metal nanoparticles with tailored morphology would be the use of pre-formed gold nanocrystals as templates, on which other metals could be grown. This would allow not only a tight control over the growth, and morphology of the nanocrystals, but also an interesting enhancement of the functionality of such nanomaterials,[4–8] the properties of which would differ from those found in similar nanostructures made of the individual constituent metals.[4–11]

In particular, various approaches have been developed to fabricate Au@Ag core–shell nanoparticles by the epitaxial growth of Ag on preformed Au nanoparticles, which were in general based on either chemical or photoinduced reduction processes.[5,9,10,12] The former often make use of a weak reducing agent, such as ascorbic acid or hydroxylamine, so that the reduction takes place exclusively on the surface of the metallic seed particles, which act as catalysts.[9,13–16, 34] However, this can only be achieved within a narrow pH range so that homogeneous nucleation of Ag nanoparticles in solution is avoided.

Herein, we describe a simple and rapid method to grow silver on single-crystal Au nanorods, resulting in single-crystal core–shell Au@Ag nanoparticles with tailored morphology, ranging from nanorods all the way to spheres, through octahedrons, and thereby giving rise to a remarkable control over the optical response spanning the whole visible range and into the near IR.

The growth method is based on the use of hydroquinone as reducing agent. Although the preparation of silver nanoparticles using hydroquinone has been previously reported, this typically resulted in a rather poor control over shape and size.[17,18] Additionally, hydroquinone has also been used to grow thin silver shells on gold nanoparticles as a means to amplify their scattering properties, but this was restricted to very thin shells on small spherical particles.[19,20] However, we demonstrate here that these processes can be utilized in a much more controlled manner, thus allowing exquisite morphology control. Based on our previous experience on the reshaping of single-crystal gold nanorods into octahedrons,[21] we decided to explore the coating of the same type of nanorods with silver, so as to tune the morphology of the resulting core–shell particles. Interestingly, we found that silver grows preferentially on the lateral facets of the Au nanorods, so that, indeed complete reshaping of the initial rods into Au@Ag octahedrons and even spheres was achieved, which might be related to the prior capping agent exchange from cetyltrimethylammonium bromide (CTAB) to methoxy-poly(ethylene glycol)-thiol (mPEG-SH). Detailed analysis of the optical response of a number of Au@Ag nanoparticles with varying Ag shell and thickness, as well as theoretical modeling by means of the boundary element method (BEM),[22,23] revealed that this system provides an excellent opportunity to gradually change the localized surface plasmon resonance (LSPR) frequency from the NIR, all the way through the complete visible range.

The synthetic method is thus based on the use of hydroquinone (HQ) as a mild reducing agent to reduce Ag^+ ions selectively onto the gold nanorods surface. Single-crystal Au nanorods with an average aspect ratio of 4.6 ± 0.6 ($61.7 \pm 5.2 \times 13.5 \pm 1.2$ nm) were prepared by standard seeded growth in CTAB[24] (see the Experimental Section in the

[a] A. Sánchez-Iglesias, E. Carbó-Argibay, Dr. A. Glaria, Dr. B. Rodríguez-González, Dr. J. Pérez-Juste, Dr. I. Pastoriza-Santos, Prof. Dr. L. M. Liz-Marzán
Departamento de Química Física
and Unidad Asociada CSIC-Universidade de Vigo
36310 Vigo (Spain)
Fax: (+34) 986812556
E-mail: pastoriza@uvigo.es

Supporting information for this article is available on the WWW under http://dx.doi.org/10.1002/chem.201000144.

Supporting Information for details). Prior to silver growth, CTAB was exchanged with mPEG-SH to preserve colloidal stability during transfer into a phosphate buffer solution, which was essential to maintain a constant pH value of 7.4 (see below). Growth of the Ag shell was then carried out at room temperature by reducing silver ions with HQ in the buffered solution of Au nanorods. Because the redox potential of hydroquinone varies with pH,[25] and H^+ is involved in the quinone/hydroquinone redox reaction, it is necessary to monitor the pH during the process. Thus, while at pH 7.4 or above, the HQ redox potential[18] is sufficient to overcome that of silver, both in the presence and in the absence (only for $[Ag^+] > 16$ mM) of Au nanoparticles, at pH values below 7 it becomes less negative and incomplete or no reduction takes place, even when Au nanoparticles are present (data not shown). It should be noted that excess hydroquinone ($[HQ]/[Ag^+] = 1:1$, rather than the 1:2 stoichiometric ratio), was used for all experiments to ensure complete Ag reduction.

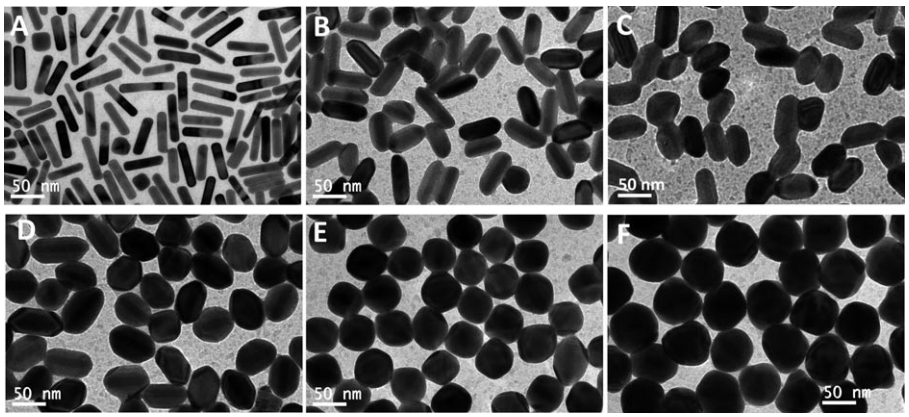

Figure 1. TEM images of Au nanorods coated with different amounts of Ag. The corresponding $[Ag^+]/[Au]$ ratios (R) are: A) 0, B) 2, C) 4, D) 6, E) 8, and F) 16. The average aspect ratios of the Au nanorods and the various Au@Ag core–shell nanoparticles are 4.6 ± 0.6 (A), 2.5 ± 0.3 (B), 1.8 ± 0.2 (C), 1.5 ± 0.2 (D), 1.2 ± 0.2 (E), and approximately 1 (F).

From the synthetic point of view, this method offers important advantages over previously reported procedures, and this is why full morphological control can be achieved from very thin to rather thick shells. On one hand, the evolution of the UV/Vis-NIR spectra during Ag^+ reduction (see Figure S1 in the Supporting Information) showed that the process can be completed within only 2–3 min, even being carried out at room temperature. Additionally, no homogeneous nucleation of free Ag nanoparticles was observed, as indicated by the lack of changes in the UV/Vis spectra between 350 and 450 nm, even after washing by centrifugation. However, we found that an additional stabilizer was necessary upon silver growth to avoid aggregation. The positive polyelectrolyte polyethylenimine (PEI) was found to be the most suitable choice, providing the colloids with sufficient electrostatic stability (see the Experimental Section in the Supporting Information).

Transmission electron microscopy was used to characterize the size and shape of the particles obtained upon reduction of different amounts of silver (measured through the molar ratio between reduced Ag^+ and Au atoms in the Au nanorod seeds, R). Although both gold and silver show face-centered cubic (FCC) crystal structures, and their lattice constants are almost identical (0.40789 nm and 0.40861 nm for Au and Ag, respectively), the core–shell structure can be easily observed from TEM images, in particular for the thinner Ag coatings, because Au and Ag atoms present different electron density, thus providing sufficient contrast. The representative TEM images shown in Figure 1 and Figure S2 in the Supporting Information confirm that thicker Ag shells were grown as R was increased. However, the images also show that the Ag shell thickness is not uniform around the particles. Careful analysis of the TEM images revealed that the growth of Ag on the Au nanorod seeds takes place preferentially at the lateral sides, so that the particles become thicker, resulting in their morphological evolution. More quantitatively, the aspect ratio of the particles gradually decreased after Ag coating, from 4.6 ± 0.6 through various values (2.5 ± 0.3, 1.8 ± 0.2, 1.5 ± 0.2, 1.2 ± 0.2, for R values of 2, 4, 6 and 8, respectively), down to about 1.0 when R was sufficiently high (16). Additional details concerning the dimensions of the nanoparticles can be found in Table S1 in the Supporting Information.

Indeed, the trend observed in the TEM images resembles the morphological evolution previously reported during the growth of single-crystal Au nanorods induced by Au reduction in a *N*,*N*-dimethylformamide (DMF) solution containing poly(vinylpyrrolidone) (PVP).[21] In that process, the gold rods gradually evolved into octahedrons through a gradual decrease in their aspect ratio, which resulted from the faster growth of certain crystallographic facets to minimize the total surface energy. However, the observed preferential growth did not follow the general sequence of surface energies for the different Au fcc crystal planes, which was explained on the basis of alterations in surface energy due to PVP adsorption. In the present case, we did not use PVP as the stabilizer, but rather mPEG-SH. It has been reported that molecules containing thiol groups, such as cysteine or glutathione, preferentially bind to the ends of Au nanorods, thereby completely blocking their longitudinal growth.[26–28] Therefore, a similar behavior for mPEG-SH might be behind the negligible change in the length of the nanorods during silver growth (except for $R = 16$, see Table S1 in the Supporting Information). As in our previous work (with

Au), whereas at low Ag^+ concentrations the obtained particles maintained a rodlike morphology, at high R values the particles become more rounded, resembling rounded octahedrons.

The octahedral morphology of the core–shell nanoparticles obtained with R = 8 was confirmed by tilting experiments in the TEM, coupled to selected-area electron diffraction (SAED) for the different particle orientations (Figure 2). Regardless of the particle orientation, the Au nanorod core within the nanoparticles was clearly distinguishable. The nanoparticle shapes (hexagonal, rectangular, and rhombic), shown in Figure 2, indeed correspond to an octahedron oriented in the [111] (Figure 2a), [112] (Figure 2c), or [110] (Figure 2e) zone axes (see cartoons of octahedron projections in Figure S4 in the Supporting Information), respectively, as revealed by the corresponding SAED patterns (Figure 2b, 2d, and 2f). Additionally, the SAED analysis also seems to indicate that the Au@Ag particle is a single crystal, even though faint forbidden spots and splitted spots (Figure 2b and 2d) or a "grid-like" pattern containing streaks (Figure 2f and Figure S5c in the Supporting Information) are present in the diffraction patterns. The origin of all of these effects is likely due to the presence the lamellar twins,[29,30] which can be clearly identified at the boundaries of the particle oriented in the [110] zone axis (Figure 2e and Figure S5 in the Supporting Information), in the form of asymmetric contrast distributions. Besides, high-resolution TEM (HRTEM) analysis revealed (see Figure S5 in the Supporting Information) the twinning plane as {111} and the twinning axis as <110>. It is also worth pointing out here that twin intersections were observed (see Figure 2e and Figure S5 in the Supporting Information) in the direction perpendicular to the nanorod core, but not at the positions of the gold nanorod tips, which might again be explained in terms of the blocking effect of mPEG-SH molecules inhibiting Ag growth. Finally, the crystallographic direction <100> for the particle oriented in the [110] zone axis coincides with that previously reported for single-crystal Au nanorods,[21,31] which is a strong indication of the epitaxial growth of silver atoms onto the Au nanorod seeds.

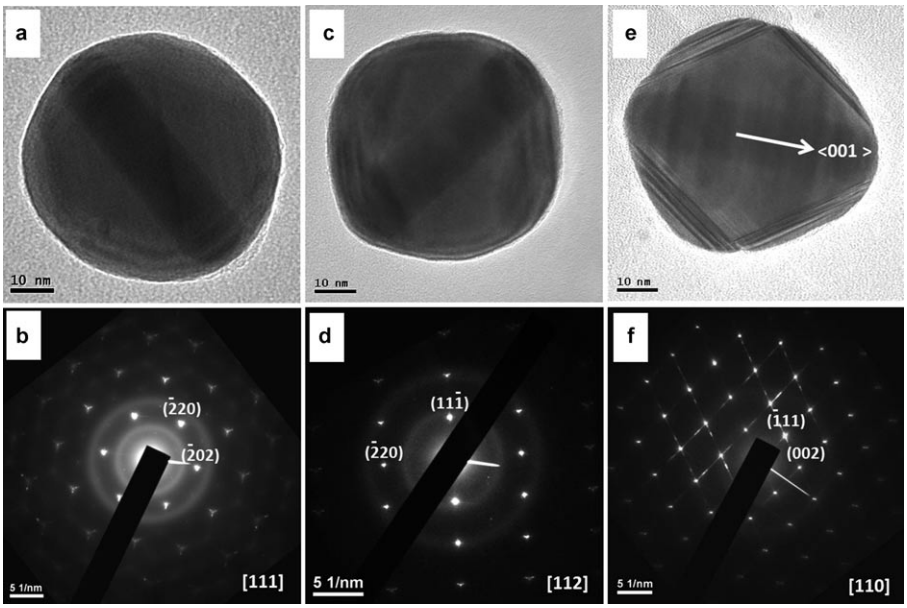

Figure 2. TEM images (upper panel) and corresponding diffraction patterns (lower panel) for Au@Ag rounded octahedrons oriented in different zone axes: (a, b) [111], (c, d) [112], (e, f) [110]. Note that the Au nanorod core is clearly discerned. The contrast differences observed at the particle edges in (e) reveal the presence of lamellar twins. Electron diffraction rotations (in b, d, and f) were compensated.

Additional confirmation of the (rounded) octahedral morphology of the coating is the projection image for a nanoparticle in the [100] zone axis shown in Figure 3a. In this image, both a square cross-section for the Au@Ag nanoparticle and an octagonal cross-section for the Au nanorod core can be identified. However, a complicated electron contrast is observed within the shell, probably due to the combination of equal-thickness fringes and lamellar twinning effects, which makes the resolution of the electron diffraction pattern extremely challenging. The main spots of the nanobeam diffraction (NBD) pattern in Figure 3b arise from the silver shell, but some splitting can be seen, probably due to contributions from both the gold nanorod and the external lamellar twins. Finally, since both core and shell present the same <100> crystallographic direction (Figure 3b, c), epitaxial growth of the Ag shell on the Au nanorod can be assigned. Although so far we have proposed that these particles grow as single crystals until forming a perfect octahedron with eight {111} facets, Ag growth ultimately leads to the development of lamellar twins and therefore to the deviation from the pure single-crystal octahedron into a more rounded morphology. A final element of characterization was carried out through detailed STEM-XEDS (scanning transmission electron microscopy coupled to X-ray energy-dispersive spectroscopy) and STEM-HAADF (STEM equipped with a high-angle annular dark-field detector) analysis, so as to confirm the composition of the core–shell particles (see Figure S6 in the Supporting Information). Both the STEM-XEDS mapping providing elemental distribution (using Au Lα and Ag Lα lines), and the STEM-HAADF image showing mass-thick-

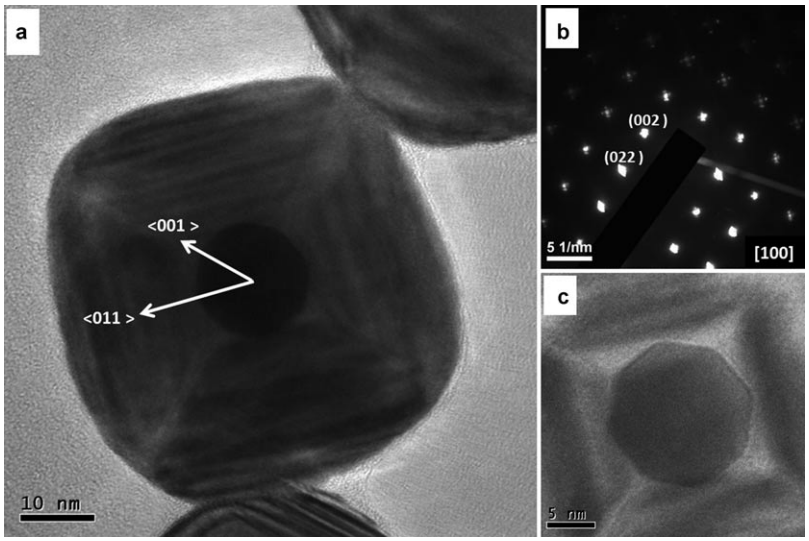

Figure 3. a) TEM image of an Au@Ag core–shell nanoparticle oriented in the [100] zone axis. The main crystallographic directions for the silver shell are indicated. b) Nanobeam diffraction pattern obtained at the center of the particle shown in a. c) Enlarged image of the nanoparticle center revealing the octagonal cross-section of the Au nanorod core.

ness contrast, nicely confirmed that the particles are made of an inner Au nanorod core surrounded by a Ag shell.

As expected, the growth of Ag on Au nanorods dramatically affects their extinction spectra, as shown in Figure 4a. The origin of such strong variations can be assigned to the differences between the dielectric functions of Ag and Au, which result in a variation of the effective dielectric function of the core–shell nanoparticles, increasing with the amount of deposited silver, as has been shown earlier for core–shell spheres.[15] However, one should also consider that the preferential growth of Ag on the lateral facets of the Au rods leads to a gradual decrease in the overall aspect ratio, which also affects the optical properties. It should be noted that all the spectra in Figure 4a correspond to colloids containing the same number of particles, but in which different amounts of silver have been used for the growth (see Experimental Section in the Supporting Information). For R up to 6, the particles preserve a rodlike morphology, and therefore the longitudinal and transverse LSPR bands can still be distinguished, while they (initially centered at 853 nm and 511 nm) are both drastically blue-shifted and acquire higher intensities (because of both the higher extinction cross-section of silver and the increase in particle volume). Interestingly, while the longitudinal LSPR gradually blue-shifts, the transverse LSPR abruptly blue-shifts when Ag is initially deposited but it subsequently slowly red-shifts when the shell becomes increasingly thicker, as a consequence of the increase in particle width.[17] On the other hand, for R larger than 6, the two initial modes merge into one intense LSPR band because the Au@Ag core–shell nanostructures present aspect ratios close to 1.0 (see Figure 1e, f and Table S1 in the Supporting Information).

Confirmation of the validity of these experimental data was obtained through modeling, by means of the boundary element method (BEM).[22,23] The BEM can be readily applied to objects with arbitrary shapes, but it is particularly advantageous when an axial rotation symmetry can be defined.[32] Further details on the calculation method are provided in the Supporting Information. Since particles with different amounts of deposited Ag present obvious geometrical differences, two different geometrical models were devised on the basis of the shapes observed in the TEM images. Thus, whereas for Au@Ag core–shell particles with R below 6 two concentric cylinders with rounded tips were modeled, for higher R the model was a rounded cylinder inside a bicone (bicones have proven suitable models for bipyramids).[32] The geometrical models are schematically depicted in Figure 4b. The spectra calculated by using these simplified models were in excellent agreement with the experimental measurements, as can be observed in Figure 4. In general, the same trend in terms of

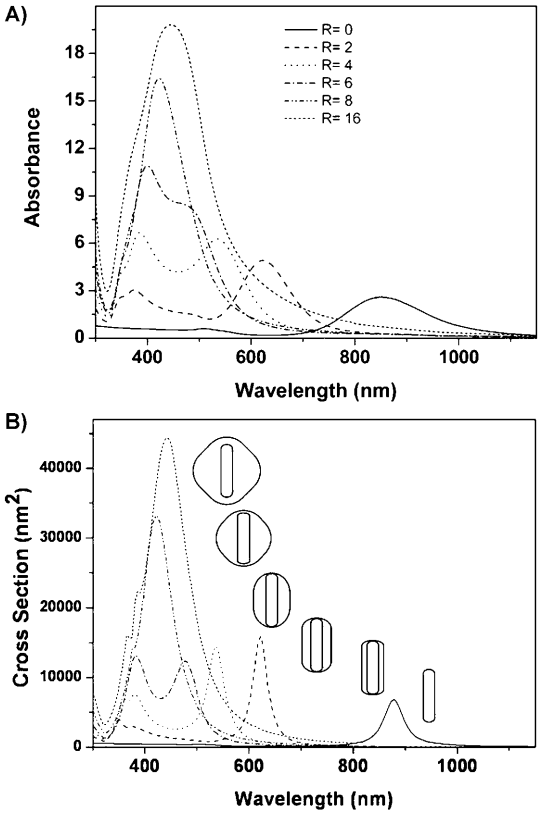

Figure 4. A) UV/Vis-NIR spectra for aqueous dispersions of Au nanorods coated with different amounts of Ag, as labeled. B) Calculated BEM spectra for Au@Ag geometrical models as depicted within the graph.

band shifts and intensities is observed though, as expected, the experimental spectra are wider than the calculated ones, due to polydispersity in the real colloids. Polydispersity is also responsible for the differences observed between calculated and experimental spectra for $R=6$, where TEM images (Figure 1d and Figure S2 in the Supporting Information) show a small percentage of particles with an aspect ratio close to 1, which contribute to the apparently increased intensity of the transverse LSPR mode of particles with higher aspect ratio.

Finally, additional calculations were carried out to elucidate the actual contribution of the Ag shell on the optical response of the coated particles. To this end, the calculated spectra from Figure 4b were compared (see Figure S3 in the Supporting Information) with calculated spectra for pure Ag nanoparticles with the same external geometry and dimensions. Interestingly, while the spectral features are clearly different for nanorods made of pure Au or Ag, as expected from their different dielectric functions, the differences (LSPR band positions and intensity) become gradually less evident as more Ag is deposited on the Au nanorod surface. Actually, the results indicate that Au nanorods coated with a thin shell of Ag already present optical properties that are closer to those of a pure Ag rod than to a pure Au rod with the same dimensions. This can be explained taking into account that the surface plasmon resonances are phenomena that are mainly localized at particle surfaces and therefore even a thin Ag shell will have a strong influence on the effective dielectric function of the core–shell nanostructure. The strong influence of a metallic thin coating on the optical response of Au nanorods was previously reported.[33] Thus, since the synthesis of Ag nanorods with a controlled aspect ratio is still an issue, coating Au nanorods with Ag shells of suitable thickness might indeed become a viable alternative to producing particles with the desired optical response.

In summary, Au@Ag core–shell nanostructures with controlled morphology can be fabricated at room temperature through the selective reduction of Ag^+ ions onto the surface of Au nanorods, using hydroquinone as a reducing agent. The presence of SH-PEG preferentially bound at the Au nanorod tips seems to completely block Ag growth in the longitudinal direction, thereby inducing a notable reshaping of the particles, with a subsequent decrease of aspect ratio, and ultimately leading to single-crystal octahedrons, which get rounded through lamellar twinning upon further reduction. The morphology and thus the optical properties of these core–shell nanostructures can be finely tuned by controlling the amount of Ag grown on the particles surface, and the optical properties of Au@Ag core–shell particles can be successfully modeled by using the BEM for models based on either concentric capped cylinders or a cylinder surrounded by a bicone. This system has also allowed us to demonstrate that growth of a thin Ag shell on Au nanorods is sufficient to obtain particles with optical properties similar to those expected for pure Ag nanoparticles with the same morphology.

Acknowledgements

E.C.-A. acknowledges MiCInn for an F.P.U. scholarship. This work was supported by the Spanish Ministerio de Ciencia e Innovación (MAT2007-62696) and the EU (INGENIOUS, grant number CP-248236).

Keywords: core–shell nanostructures · epitaxial growth · gold · nanostructures · silver

[1] I. Pastoriza-Santos, L. M. Liz-Marzán, *Adv. Funct. Mater.* **2009**, *19*, 679–688.
[2] B. Wiley, Y. Sun, B. Mayers, Y. Xia, *Chem. Eur. J.* **2005**, *11*, 454–563.
[3] Y. Xia, Y. Xiong, B. Lim, S. E. Skrabalak, *Angew. Chem.* **2009**, *121*, 62–108; *Angew. Chem. Int. Ed.* **2009**, *48*, 60–103.
[4] B. Lim, J. Wang, P. H. C. Carmargo, M. Jiang, M. J. Kim, Y. Xia, *Nano Lett.* **2008**, *8*, 2535–2540.
[5] S. Xing, L. H. Tan, T. Chen, Y. Yang, H. Chen, *Chem. Commun.* **2009**, 1653–1654.
[6] Y. J. Xiang, X. C. Wu, D. F. Liu, X. Y. Jiang, W. G. Chu, Z. Y. Li, Y. Ma, W. Y. Zhou, S. S. Xie, *Nano Lett.* **2006**, *6*, 2290–2294.
[7] F.-R. Fan, D.-Y. Liu, Y.-F. Wu, S. Duan, Z.-X. Xie, Z.-Y. Jiang, Z.-Q. Tian, *J. Am. Chem. Soc.* **2008**, *130*, 6949–6951.
[8] M. Grzelczak, B. Rodríguez-González, J. Pérez-Juste, L. M. Liz-Marzán, *Adv. Mater.* **2007**, *19*, 2262–2266.
[9] B. Rodríguez-González, A. Burrows, M. Watanabe, C. J. Kiely, L. M. Liz-Marzán, *J. Mater. Chem.* **2005**, *17*, 1755–1759.
[10] C. Xue, J. E. Millstone, S. Li, C. A. Mirkin, *Angew. Chem.* **2007**, *119*, 8588–8591; *Angew. Chem. Int. Ed.* **2007**, *46*, 8436–8439.
[11] S. E. Habas, H. Lee, V. Radmilovic, G. A. Somorjai, P. Yang, *Nat. Mater.* **2007**, *6*, 692–697.
[12] M. Tsuji, R. Matsuo, P. Jiang, N. Miyamae, D. Ueyama, M. Nishio, S. Hikino, H. Kumagae, K. Sozana N. Kamarudin, X.-L. Tang, *Cryst. Growth Des.* **2008**, *8*, 2528–2536.
[13] C. S. Ah, S. D. Hong, D.-J. Jang, *J. Phys. Chem. B* **2001**, *105*, 7871–7873.
[14] L. Lu, H. Wang, Y. Zhou, S. Xi, H. Zhang, J. Hu, B. Zhao, *Chem. Commun.* **2002**, 144–145.
[15] M. Liu, P. Guyot-Sionnest, *J. Phys. Chem. B* **2004**, *108*, 5882–5888.
[16] Y. Xiang, X. Wu, D. Liu, Z. Li, W. Chu, L. Feng, K. Zhang, W. Zhou, S. Xie, *Langmuir* **2008**, *24*, 3465–3470.
[17] M. A. Pérez, R. Moiraghi, E. A. Coronado, V. A. Macagno, *Cryst. Growth Des.* **2008**, *8*, 1377–1383.
[18] S. T. Gentry, S. J. Fredericks, R. Krchnavek, *Langmuir* **2009**, *25*, 2613–2621.
[19] D.-K. Lim, I.-J. Kim, J.-M. Nam, *Chem. Commun.* **2008**, 5312–5314.
[20] X. Xu, D. G. Georganopoulou, H. D. Hill, C. A. Mirkin, *Anal. Chem.* **2007**, *79*, 6650–6654.
[21] E. Carbó-Argibay, B. Rodríguez-González, J. Pacifico, I. Pastoriza-Santos, J. Pérez-Juste, L. M. Liz-Marzán, *Angew. Chem.* **2007**, *119*, 9141–9145; *Angew. Chem. Int. Ed.* **2007**, *46*, 8983–8987.
[22] F. J. García de Abajo, A. Howie, *Phys. Rev. Lett.* **1998**, *80*, 5180–5183.
[23] F. J. García de Abajo, A. Howie, *Phys. Rev. B* **2002**, *65*, 115418–1–17.
[24] B. Nikoobakht, M. A. El-Sayed, *Chem. Mater.* **2003**, *15*, 1957–1962.
[25] M. M. Walczak, D. A. Dryer, D. D. Jacobson, M. G. Foss, N. T. Flynn, *J. Chem. Educ.* **1997**, *74*, 1195–1197.
[26] K. G. Thomas, S. Barazzouk, B. I. Ipe, S. T. S. Joseph, P. V. Kamat, *J. Phys. Chem. B* **2004**, *108*, 13066–13068.
[27] J.-Y. Chang, H. M. Wu, H. Chen, Y.-C. Ling, W. H. Tan, *Chem. Commun.* **2005**, 1092–1094.
[28] X. Kou, S. Zhang, Z. Yang, C.-K. Tsung, G. D. Stucky, L. Sun, J. W. , C. Yan, *J. Am. Chem. Soc.* **2007**, *129*, 6402–6404.
[29] D. T. Smith, L. D. Marks, *J. Crystal Growth* **1981**, *54*, 433.

[30] L. C. Gontard, R. E. Dunin-Borkowski, M. H. Gass, A. L. Bleloch, D. Ozkaya, *J. Electron Microsc.* **2009**, *58*, 167–174.
[31] Z. L. Wang, M. B. Mohamed, S. Link, M. A. El-Sayed, *Surf. Sci.* **1999**, *440*, 809–814.
[32] A. Sánchez-Iglesias, I. Pastoriza-Santos, J. Pérez-Juste, B. Rodríguez-González, F. J. García de Abajo L. M. Liz-Marzán, *Adv. Mater.* **2006**, *18*, 2529–2534.
[33] M. Grzelczak, J. Pérez-Juste, F. J. García de Abajo, L. M. Liz-Marzán, *J. Phys. Chem. C* **2007**, *111*, 6183–6188.
[34] During the reviewing of this paper, similar related work appeared, see: E. C. Cho, P. H. C. Camargo, Y. Xia, *Adv. Mater.* **2010**, *22*, 744–748.

Received: October 22, 2009
Revised: January 19, 2010
Published online: April 6, 2010

